OPEN ACCESS Freely available online

PLOS ONE

Construction and Application of Elastin Like Polypeptide Containing IL-4 Receptor Targeting Peptide

Vijaya Sarangthem[1], Eun A. Cho[1], Sang Mun Bae[1], Thoudam Debraj Singh[2], Sun-Ji Kim[1], Soyoun Kim[1], Won Bae Jeon[3], Byung-Heon Lee[1], Rang-Woon Park[1]*

1 Department of Biochemistry and Cell Biology, Cell & Matrix Research Institute, Kyungpook National University, School of Medicine, Daegu, Republic of Korea, **2** Department of Nuclear Medicine, Kyungpook National University, School of Medicine, Daegu, Republic of Korea, **3** Division of NanoBioTechnology, Laboratory of Biochemistry and Cellular Engineering, Daegu Gyeongbuk Institute of Science and Technology, Daegu, Republic of Korea

Abstract

Various human solid tumors highly express IL-4 receptors which amplify the expression of some of anti-apoptotic proteins, preventing drug-induced cancer cell death. Thus, IL-4 receptor targeted drug delivery can possibly increase the therapeutic efficacy in cancer treatment. Macromolecular carriers with multivalent targeting moieties offered great advantages in cancer therapy as they not only increase the plasma half-life of the drug but also allow delivery of therapeutic drugs to the cancer cells with higher specificity, minimizing the deleterious effects of the drug on normal cells. In this study we designed a library of elastin like polypeptide (ELP) polymers containing tumor targeting AP1 peptide using recursive directional ligation method. AP1 was previously discovered as an atherosclerotic plaque and breast tumor tissue homing peptide using phage display screening method, and it can selectively bind to the interleukin 4 receptor (IL-4R). The fluorescently labeled $[AP1\text{-}V_{12}]_6$, an ELP polymer containing six AP1 enhanced tumor-specific targeting ability and uptake efficiency in H226 and MDA-MB-231 cancer cell lines *in vitro*. Surface plasmon resonance analysis showed that multivalent presentation of the targeting ligand in the ELP polymer increased the binding affinity towards IL-4 receptor compared to free peptide. The binding of $[AP1\text{-}V_{12}]_6$ to cancer cells was remarkably reduced when IL-4 receptors were blocked by antibody against IL-4 receptor further confirmed its binding. Importantly, the Cy5.5-labeled $[AP1\text{-}V_{12}]_6$ demonstrated excellent homing and longer retention in tumor tissues in MDA-MB-231 xenograft mouse model. Immunohistological studies of tumor tissues further validated the targeting efficiency of $[AP1\text{-}V_{12}]_6$ to tumor tissue. These results indicate that designed $[AP1\text{-}V_{12}]_6$ can serve as a novel carrier for selective delivery of therapeutic drugs to tumors.

Citation: Sarangthem V, Cho EA, Bae SM, Singh TD, Kim S-J, et al. (2013) Construction and Application of Elastin Like Polypeptide Containing IL-4 Receptor Targeting Peptide. PLoS ONE 8(12): e81891. doi:10.1371/journal.pone.0081891

Editor: Sanjoy Bhattacharya, Bascom Palmer Eye Institute, University of Miami School of Medicine, United States of America

Received May 31, 2013; **Accepted** October 17, 2013; **Published** December 10, 2013

Copyright: © 2013 Sarangthem et al. This is an open-access article distributed under the terms of the Creative Commons Attribution License, which permits unrestricted use, distribution, and reproduction in any medium, provided the original author and source are credited.

Funding: This research was supported by the Ministry of Knowledge Economy (MEK) by grant no. RTI04-01-01 from the Regional Technology Innovation Program and R&D program of MOTIE/KEIT (10040393, Development and commercialization of molecular diagnostic technologies for lung cancer through clinical validation). The funders had no role in study design, data collection and analysis, decision to publish, or preparation of the manuscript.

Competing Interests: The authors have declared that no competing interests exist.

* E-mail: nwpark@knu.ac.kr

Introduction

Targeted macromolecular polymer carriers offer the potential of effective drug delivery by virtue of their ability to decrease the rate of drug clearance after systematic administration and improve the plasma half-life of drugs [1]. One such engineered biopolymer is elastin-like polypeptide (ELP), which is an emerging drug carrier under development for cancer therapy. In several cancer models, ELPs have already been used for targeted delivery of small molecules drugs (doxorubicin) [2,3], therapeutic peptides (c-Myc inhibitory peptide) [4] and proteins [5]. They have unique characteristics compared to other polymeric drug delivery systems, including low toxicity, good biodegradability, and biocompatibility [6,7]. ELP biopolymers are derived from the structural motif found in mammalian elastin protein, which consists of the pentapeptide repeat, Val-Pro-Gly-Xaa-Gly (VPGXG), where Xaa (“guest” residue) can be any amino acid except proline [8,9]. ELP polymers can be synthesized at the genetic level using recombinant DNA methods; thus, their sequence, composition, and molecular weight can be controlled. Accordingly, the hydrophobicity and degree of ionization can be precisely tuned for proper tissue distribution and subcellular uptake [10,11]. Moreover, the numbers of targeting peptides or specific reactive sites for drug conjugation can be incorporated at the genetic level along with the ELP sequence, which is one of the difficulties to accomplish using synthetic polymers. ELPs are soluble in aqueous solutions below their transition temperature (T_t), but hydrophobically collapse and aggregate at temperatures greater than T_t [12,13]. This inverse transition temperature is fully reversible. The transition temperature of ELP can be controlled by varying the guest residue, molecular weight and concentration [10]. Notably, ELPs can be easily expressed and purified at high yield simply by exploiting inverse temperature cycling (ITC) method [14,15].

Using phage display screening, we previously discovered an atherosclerotic plaque and breast tumor tissue homing peptide, CRKRLDRN, termed AP1 peptide that selectively binds to the interleukin -4 receptors (IL-4Rs) [16–18]. IL-4Rs are highly expressed in a wide variety of human tumors, including renal cell carcinoma, squamous cell carcinoma of the head and neck, malignant glioma, AIDS-associated Kaposi’s sarcoma and breast cancer cell lines [19–22]. It has been reported that IL-4/IL-4R interactions amplify the expression of some anti-apoptotic

proteins, including PED/PEA15 (15 kDa phosphoprotein enriched in astrocytes), cFLIP/CFLAR (CASP8 and FADD-like apoptosis regulator), and the BCL family proteins Bcl-xL and Bcl, thereby preventing drug-induced cancer cell death [23,24]. Thus, targeting the IL-4R could possibly increase the therapeutic efficacy of anticancer drugs. Even though AP1 peptide possesses high target-specificity and efficient tumor-homing, it has limitation due to easy elimination from the circulation and short half-life.

The aim of this study is to increase the stability and binding affinity of the AP1 peptide *in vivo*, and thus increase its utility, through multivalent presentation of the AP1 peptide in an ELP polymer backbone. Many studies have demonstrated that the presentation of multiple targeting moieties on a polymer backbone can improve binding avidity and specificity compared to monovalent ligand presentation [25]. Accordingly, we designed and prepared a series of an AP1 peptide containing ELP polymer using recursive directional ligation (RDL) method and analyzed the characteristics and the efficacy *in vitro* and *in vivo*. The binding specificity of $[AP1\text{-}V_{12}]_6$ polymer towards cancer cells was analyzed using confocal microscopy and flow cytometry, and *in vivo* optical imaging in a tumor xenograft mouse model. The studies have revealed that the incorporation of multivalent targeting peptide ligand into ELP polymer facilitated the greater targeting to IL-4R expressing cancer cells.

Materials and Methods

Media and cell culture

H226 (human lung cancer cells), MDA-MB-231 (human breast cancer cells), and H460 (human lung cancer cells) were obtained from American Type Culture Collection (ATCC). H226 and H460 cells were grown in RPMI-1640 (Hyclone, Thermo Scientific, Logan, UT), and MDA-MB-231 cells were grown in Dulbecco's modified Eagle's medium (DMEM) (Hyclone, Thermo Scientific) supplemented with 10% fetal bovine serum (Hyclone, Thermo Scientific) and 100 U/mL penicillin and 100 μg/mL of streptomycin (Sigma Aldrich, St. Louis, MO, USA). Cells were maintained at 37°C in a humidified atmosphere containing 5% CO_2.

Designing of monomer gene and oligomerization

Synthetic oligonucleotides encoding genes of $[VGVPG]_{14}$ and $VGRKRLDRNG[VGVPG]_{12}$ referred as V_{14} and AP1-V_{12} were designed to contain *Bam*H I and *Hin*D III compatible cohesive ends upon annealing, which allows the annealed product to be directly ligated into a *Bam*H I and *Hin*D III-cleaved pRSET B+ vector (Invitrogen, CA, USA) [26,27]. The resulting vector containing V_{14} and AP1-V_{12} were used as a monomer to synthesized $[V_{14}]_2$ and $[AP1\text{-}V_{12}]_2$. Additional rounds of RDL were performed to acquire different length $[AP1\text{-}V_{12}]_n$ polymers where n = 2, 4, 5 and 6 with different molecular weights and thermal transition characteristics. The polymers used in the study have the composition $[V_{14}]_6$ and $[AP1\text{-}V_{12}]_6$.

$[V_{14}]_6$ and $[AP1\text{-}V_{12}]_6$ proteins expression

The pET 25 b+ (Novagen, Canada, USA) expression plasmid was doubled digested with *Nde* I and *Hin*D III and purified using a gel extraction kit (ELPIS Biotech, Daejeon, Korea). The synthetic oligonucleotides 5′-TAT GAG CGG GCC GGG CTG GCC GTG CTA AA-3′ (sense) and 5′-AGC TTT TAG CAC GGC CAG CCC GGC CCG CTC A-3′ (antisense) were annealed to form double-stranded DNA containing *Nde* I, *Sfi* I, and *Hin*D III restriction sites and ligated to *Nde* I and *Hin*D III double-digested pET 25 b+ vector. After confirmation by DNA sequencing, the modified pET 25b+ vector was linearized with *Sfi* I and enzymatically dephosphorylated with CIP (New England Biolab, Ipswich, MA). The $[V_{14}]_6$ and $[AP1\text{-}V_{12}]_6$ genes were ligated to linearized, modified pET 25b+ vector and transformed into DH5α competent *E. coli* cells. Plasmids with the respective gene ligations were confirmed by restriction digestion with *Nde* I and *Hin*D III (New England Biolab), followed by gene sequencing (Macrogen Inc., Seoul, Korea).

ELP protein purification

BL21 (DE3) chemically competent *E. coli* cells (Invitrogen) were further transformed with modified pET 25b+ vector containing $[V_{14}]_6$ and $[AP1\text{-}V_{12}]_6$ gene for protein expression. Starter cultures were prepared by inoculating 10 mL of Circle grow media (MP Biomedicals, CA, USA) containing 100 μg/mL ampicillin (Sigma Aldrich, MO, USA) with the expression strain and incubating for 6 h at 37°C. Starter cultures were then inoculated into 1 L of fresh Circle grow media containing ampicillin and incubated for 12 h at 37°C. The cells were then harvested by centrifugation at 4000 rpm for 20 min at 4°C and suspended in 10 mL phosphate-buffered saline (PBS). Cells were lysed by sonication at 4°C, and ELP protein was purified using inverse transition cycling (ITC). Four rounds of ITC were performed to eliminate cell contaminants. ELP purity was checked by SDS-PAGE, followed by Coomassie blue staining (Bio-Rad, Hercules, CA). ELP concentration was measured by Cary UV-visible spectrophotometer (Agilent Technologies, CA, USA) using an extinction coefficient of 5690 M^{-1} cm^{-1} for both $[V_{14}]_6$ and $[AP1\text{-}V_{12}]_6$.

Thermal characterization

Transition temperature (T_t) of $[V_{14}]_6$ and $[AP1\text{-}V_{12}]_6$ were determined by monitoring the turbidity profile of protein solutions at wavelength 350 nm as a function of temperature using Cary UV-visible spectrophotometer equipped with temperature controller (Agilent Technologies). The absorbance was monitored from 20°C to 45°C in 1°C/min increments. The T_t of $[V_{14}]_6$ and $[AP1\text{-}V_{12}]_6$ protein were determined at a concentration of 10 μM.

Fluorophore conjugation

$[V_{14}]_6$ and $[AP1\text{-}V_{12}]_6$ proteins were labeled with Alexa Fluor 488-C5 maleimide (Invitrogen) or Alexa 680 maleimide (BioActs, Incheon, Korea) dyes, as per company's protocol.

Flow cytometry analysis

IL-4R highly expressed cancer cell lines such as H226 and MDA-MB-231 cells were used to examine the binding specificity of $[AP1\text{-}V_{12}]_6$ polymer. H460 cell was used as IL-4R negative control [28]. H226, MDA-MB-231, and H460 (2×10^5) cells were incubated with 2% BSA for 30 min at 37°C to block the nonspecific binding and further incubated with 10 μM Alexa 488-labeled AP1 peptide, $[V_{14}]_6$ and $[AP1\text{-}V_{12}]_6$ proteins for 1 h at 4°C. The cells were washed twice with PBS, suspended in 200 μL of PBS, and analyzed by flow cytometry (BD Bioscience, San Jose, CA, USA). For analysis, 10,000 events were collected for each sample and the total percentage of Alexa 488 labeled polymer bound to cells was calculated by comparing with untreated cells.

Competition assay

3×10^5 of H226 and MDA-MB-231 cells were pretreated with IL-4R antibody (R&D systems, Canada, USA) at various concentrations such as 1, 5 and 10 μg at 4°C for 1 h. The cells were then incubated with 10 μM Alexa 488 labeled $[AP1\text{-}V_{12}]_6$

for 1 h at 4°C. After washing with PBS for two times, cells were suspended with 300 µl of PBS and analyzed by flow cytometry. 10,000 events were analyzed for each sample.

Confocal Microscopy

H226, MDA-MB-231 and H460 cells were seeded on four chambered slide and grown to 80% confluence. Cells were then incubated with 10 µM Alexa 488 labeled $[V_{14}]_6$ and $[AP1\text{-}V_{12}]_6$ proteins and AP1 peptides for 1 h at 4°C and 37°C. Unbound peptides were washed out with PBS, and cells were fixed with 4% paraformaldehyde (Sigma Aldrich). Cell nuclei were stained with 4′,6-diamidino-2-phenylindole (DAPI; Sigma Aldrich), and chamber slides were mounted with anti-fade reagent (Invitrogen). Images were captured and analyzed in sequential scanning mode using a Zeiss LSM-510 Meta confocal microscope.

Cell viability and proliferation assay

5×10^3 of MDA-MB-231 cells were plated in serum containing media and incubated for 16 h. The cells were then treated with different concentration of $[AP1\text{-}V_{12}]_6$ and $[V_{14}]_6$ (1, 5, 10, 20 µM) in media for various time intervals such as 12, 24, 48, and 72 h respectively. WST-8 solution was added to each wells and further incubated for 1 h. WST-8 values (average absorbance, 450 nm) were measured at different time intervals to determine cell viability.

In order to access the effect of $[AP1\text{-}V_{12}]_6$ on IL-4 induced cell proliferation, MDA-MB-231 (2×10^3) cells were serum starved for 16 h by plating in low serum (1% FBS) with or without different concentrations of IL-4. The cells were further cultured with low serum (1% FBS) media containing different concentration of IL-4 (10, 50, 100 ng/ml) and $[AP1\text{-}V_{12}]_6$ and $[V_{14}]_6$ (10 µM) for 24, 48, and 72 h. Cell proliferation was analyzed by measuring the WST-8 absorbance at 450 nm.

Surface Plasmon Resonance (SPR) analysis

Interactions of AP1, $[V_{14}]_6$ and $[AP1\text{-}V_{12}]_6$ with the IL-4R were analyzed at 25°C using a surface plasmon resonance instrument (Reichert Life Sciences, NY, USA). IL-4Rα (CD124) (Sino Biological, Beijing, China) was immobilized by activating the carboxy methyl group on dextran-coated chips (Reichert Life Sciences) through a reaction with N-hydroxysuccinimide (Sigma Aldrich), followed by covalent bonding of the ligands to the chip surface via amide linkages and blocking of excess activated carboxyls with ethanolamine. Different concentrations of AP1 peptide (3.125 to 50 µM) and $[AP1\text{-}V_{12}]_6$ (125 nM to 1 µM) in binding buffer were allowed to flow over surfaces containing immobilized IL-4Rα (2000±400 RU) for 3 min at a rate of 25 µL/min. The sensor surface was regenerated after each association and dissociation cycle by injecting 10 mM HCl for 10 s. The interaction of ligand and analyte was analyzed using Scrabber 2 Biologic software. Binding kinetics was assessed by determining association (k_{on}), dissociation (k_{off}), and equilibrium (K_D) constants.

Animal Model

This study strictly followed the recommendations of National Institute of Health (NIH) for the Care and Use of Laboratory Animals. Animal experiments were reviewed and approved by the Committee on the Ethics of Animal Experiments of the Kyungpook National University (Permit Number: KNU 2012-124). All efforts were made for minimizing animal suffering. Female nude mice (BALB/c nude; body weight, 20±3 g; n = 5) were housed in a specific pathogen-free environment at 22±2°C, 55±5% relative humidity with light. Tumors were generated by subcutaneously injecting MDA-MB-231 cells (5×10^6 cells) into the right flank of 5-wk-old BALB/c nude female mice and allowing them to grow for 10days [17,29]. For *in vivo* analysis of tumor targeting, $[V_{14}]_6$ and $[AP1\text{-}V_{12}]_6$ were labeled with Alexa 680 (Cy5.5) at the C-terminal Cys residue of the protein. Tumor-bearing mice were anesthetized under inhalational anesthesia (1%, w/v, isofurane in 2 L oxygen), then injected with Cy5.5-labeled $[AP1\text{-}V_{12}]_6$ (n = 5) or, $[V_{14}]_6$ control (n = 5) of approximately 8 mg/kg via the tail vein. *In vivo* fluorescence images were taken at different time intervals after anesthetization (10 min, 1 h, 6 h, 12 h, and 24 h) using an eXplore Optix system (ART Advanced research technologies Inc., Montreal, Canada).

Tissue preparation

At 6 h time point, animals were euthanized with CO_2, tumors and organs were removed from a subset of animals, and *ex vivo* fluorescence images were collected. The tumor tissues were then fixed by incubating with 4% paraformaldehyde overnight and frozen for cryosectioning. Tissue slices (8-µm thick) were incubated overnight at 4°C with anti-IL-4R antibody (R&D Systems; 1:100) and then incubated for 30 min at room temperature with Alexa 488-labeled goat anti-mouse IgG secondary antibody (1:200). After staining nuclei with DAPI, sections were slide-mounted and observed under a confocal microscope.

Statistical analysis

The statistical significance was determined using Student's t-test for two groups and one-way ANOVA for comparing multiples groups. ***P<0.0001, **P<0.001, and *P<0.05 were considered as statistically significant and denoted by asterisks in the Figures.

Results

Design of $[AP1\text{-}V_{12}]_n$ genes and protein expression

We successfully constructed $[V_{12}]_n$ and $[AP1\text{-}V_{12}]_n$ gene libraries using the RDL method [11]. The ELP libraries consisted of the monomer genes repeat Val-Pro-Gly-Val-Gly with Valine at the guest residue of ELP pentapeptide (Fig. 1A), whereas the $[AP1\text{-}V_{12}]_n$ library contained modified AP1 sequence, in the N-terminal region of the ELP coding sequences (Fig. 1B). The monomer gene of $[AP1\text{-}V_{12}]_n$ was designed such that at each round of gene oligomerization by RDL, the AP1 sequence was repeated along with the ELP sequence. This iterative process yielded $[V_{12}]_n$ (Fig. S1A) and $[AP1\text{-}V_{12}]_n$ genes (Fig. S1B) with variable lengths and numbers of repeats. For subsequent *in vitro* and *in vivo* studies, we chose $[AP1\text{-}V_{12}]_6$ containing six AP1 sequence repeats as the target-specific polymer and $[V_{14}]_6$ as the non-targeting polymer control. For successful expression, $[AP1\text{-}V_{12}]_6$ and $[V_{14}]_6$ were ligated into a modified pET25b+ vector containing the trailer sequence WPC, providing a cysteine residue for conjugation of fluorophore or drug (Fig. S1C-E). The SGPG[VGRKRLD-RNG$(VGVPG)_{12}]_6$WPC and SGPG$[(VGVPG)_{14}]_6$WPC proteins were purified using the ITC method; the total yield was ~20 mg/L. After four rounds of ITC, SDS-PAGE followed by Coomassie blue staining showed that $[AP1\text{-}V_{12}]_6$ and $[V_{14}]_6$ were approximately ~37 kDa and ~35 kDa in size, respectively, with minimal contamination (Fig. 2A).

Thermal characterization

The T_t of $[AP1\text{-}V_{12}]_6$ and $[V_{14}]_6$ proteins were characterized at a concentration of 10 µM in PBS. The turbidity profiles were determined by measuring optical density at 350 nm (OD_{350}) as function of temperature in 1°C min^{-1} increments. The T_t, defined

A ELP sequences

$[VGVPG]_{14}$

↓ *Bam*HI ↓ *Eco*RI ↓ *Pfl*MI
5'-G ATCCTG AATTC ATG GGC CAC GGC GTG GGT GTT CCG GGC GTA GGT
M G H G V G V P G V G

GTC CCA GGT GTG GGC GTA CCG GGC GTT GGT GTT CCT GGT GTC GGC
V P G V G V P G V G V P G V G

GTG CCG GGC GTA GGT GTC CCA GGT GTG GGC GTG CCG GGC GTG GGT
V P G V G V P G V G V P G V G

GTT CCG GGC GTA GGT GTC CCA GGT GTG GGC GTA CCG GGC GTT GGT
V P G V G V P G V G V P G V G

GTT CCT GGT GTC GGC GTG CCG GGC GTA GGT GTC CCA GGT GTG GGC
V P G V G V P G V G V P G V G
↓ *Bgl*II ↓*Hin*DIII
GTG CCG GGC TGG CTT TAAA-3'
V P G W

B AP1-ELP sequence

$VGRKRLDRNG[VGVPG]_{12}$

↓ *Bam*HI ↓ *Eco*RI ↓ *Pfl*MI
5'-G ATCCTG AATTC ATG GGC CAC GGC GTG GGT CGT AAG CGT CTT GAT
M G H G V G R K R L D

CGG AAT GCC GTC GGT GTA CCG GGC GTT GGT GTT CCT GGT GTC GGC
R N G V G V P G V G V P G V G

GTG CCG GGC GTA GGT GTC CCA GGT GTG GGC GTG CCG GGC GTG GGT
V P G V G V P G V G V P G V G

GTT CCG GGC GTA GGT GTC CCA GGT GTG GGC GTA CCG GGC GTT GGT
V P G V G V P G V G V P G V G

GTT CCT GGT GTC GGC GTG CCG GGC GTA GGT GTC CCA GGT GTG GGC
V P G V G V P G V G V P G V G
↓ *Bgl*II ↓*Hin*DIII
GTG CCG GGC TGG CTT TAAA-3'
V P G W

Figure 1. Monomer genes of V_{14} and AP1-V_{12}. (A) $[VGVPG]_{14}$ and (B) $VGRKRLDRNG[VGVPG]_{12}$ monomeric genes and their corresponding polypeptide sequences.
doi:10.1371/journal.pone.0081891.g001

as the temperature at which turbidity in the protein solution reached 50%, was in the range of 37°C to 39°C for $[AP1\text{-}V_{12}]_6$ and 26°C to 28°C for and $[V_{14}]_6$ (Fig. 2B). Incorporation of the hydrophilic AP1 sequence into the ELP gene increased the T_t compared to the ELP control [30]. We observed that the inverse transition of the polymer $[AP1\text{-}V_{12}]_6$ is just above the physiological body temperature, which is preferable for clinical applications.

In vitro cell binding of $[AP1\text{-}V_{12}]_6$ polymer

To study binding efficiency, we labeled the C-terminal Cys residue of $[AP1\text{-}V_{12}]_6$ and $[V_{14}]_6$ proteins with Alexa 488. FACS analysis confirmed that the cell-binding capacity of the targeted $[AP1\text{-}V_{12}]_6$ polymer in H226 (Fig. 3A, B) and MDA-MB-231 cells (Fig. 3C, D) after a 1-h incubation at 4°C was higher than that of the non-targeted $[V_{14}]_6$ polymer ($P<0.0001$). Both non-targeted $[V_{14}]_6$ and targeted $[AP1\text{-}V_{12}]_6$ polymers showed significantly lower binding towards H460 cells (Fig. 3E, F). For the $[AP1\text{-}V_{12}]_6$ polymer, cell attachment was 5.9±1.6 fold higher in H226 cells and 5.6±1.3 fold higher in MDA-MB-231 cells compared to H460 cells. In addition, the AP1 peptide showed 4.2±1.8 and 3.4±1.1 folds higher binding to H226 and MDA-MB-231 cells than to H460 cells. Thus, the $[AP1\text{-}V_{12}]_6$ polymer exhibited 1.7 and 2.2 fold higher cell-binding capacity in H226 ($P<0.0001$) and MDA-MB-231($P<0.05$) cells than the targeting AP1 peptide

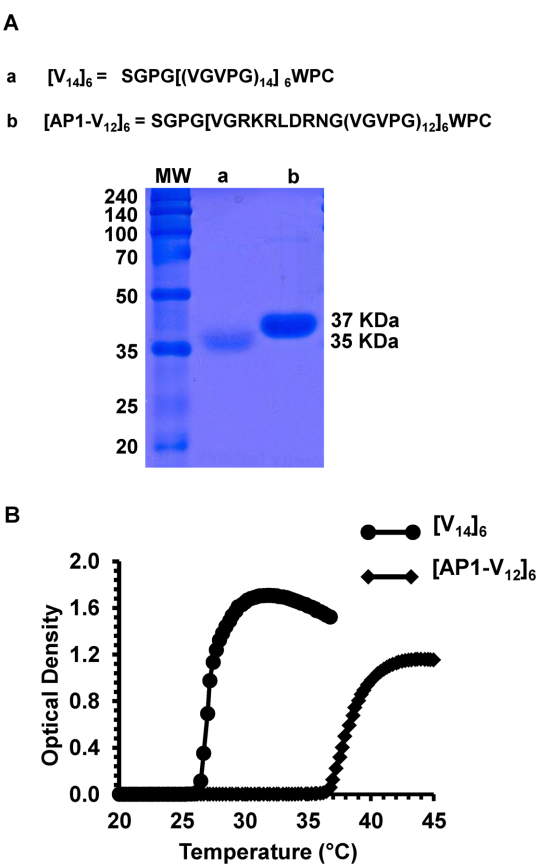

Figure 2. Protein expression and thermal characterization. (A) Polypeptide sequences of (a) $[V_{14}]_6$ and (b) $[AP1\text{-}V_{12}]_6$, expressed proteins were visualized by Coomassie Blue staining after SDS-PAGE analysis. Left lane: protein molecular weight marker (in kDa). Expected sizes of $[V_{14}]_6$ (~35 kDa) and $[AP1\text{-}V_{12}]_6$ (~37 kDa) are indicated on the right. (B) The turbidity profiles of $[V_{14}]_6$ and $[AP1\text{-}V_{12}]_6$ protein verses OD_{350} as a function of temperature (increased at a rate of 1°C min^{-1}) were obtained.
doi:10.1371/journal.pone.0081891.g002

alone. Our results suggested that multivalent presentation of the AP1 sequence in the $[AP1\text{-}V_{12}]_6$ polymer allowed greater accumulation on cells compared to the AP1 peptide.

The IL-4R dependence of $[AP1\text{-}V_{12}]_6$ polymer binding to tumor cells was further confirmed using competition assays. The binding of tumor cells by $[AP1\text{-}V_{12}]_6$ polymer was remarkably reduced in a concentration-dependent manner by pre-incubation with different concentrations (1, 5 and 10 μg/mL) of anti-IL-4R antibody (Fig. 3 G, H).

Cellular localization of $[AP1\text{-}V_{12}]_6$ polymer and affinity for IL-4R

The cellular localization of $[AP1\text{-}V_{12}]_6$ polymer at different temperatures were further confirmed by confocal microscopic imaging, which clearly revealed that $[AP1\text{-}V_{12}]_6$ polymer and AP1 peptide accumulated more efficiently to the cell surface of H226 (Fig. 4A) and MDA-MB-231 (Fig. S2A) cells at 4°C compared to H460 cells (Fig. S3A). $[AP1\text{-}V_{12}]_6$ polymer was well internalized when incubated at 37°C whereas no uptake was seen in case of $[V_{14}]_6$ polymer in both H226 (Fig. 4B) and MDA-MB-231 cells (Fig. S2B). Both non-targeted $[V_{14}]_6$ and targeted $[AP1\text{-}V_{12}]_6$ polymers have shown lower cell binding and uptake in case of IL-4R negative H460 cells (Fig. S3A, B). Thus, these results indicated that cellular uptake of $[AP1\text{-}V_{12}]_6$ polymers were not due to

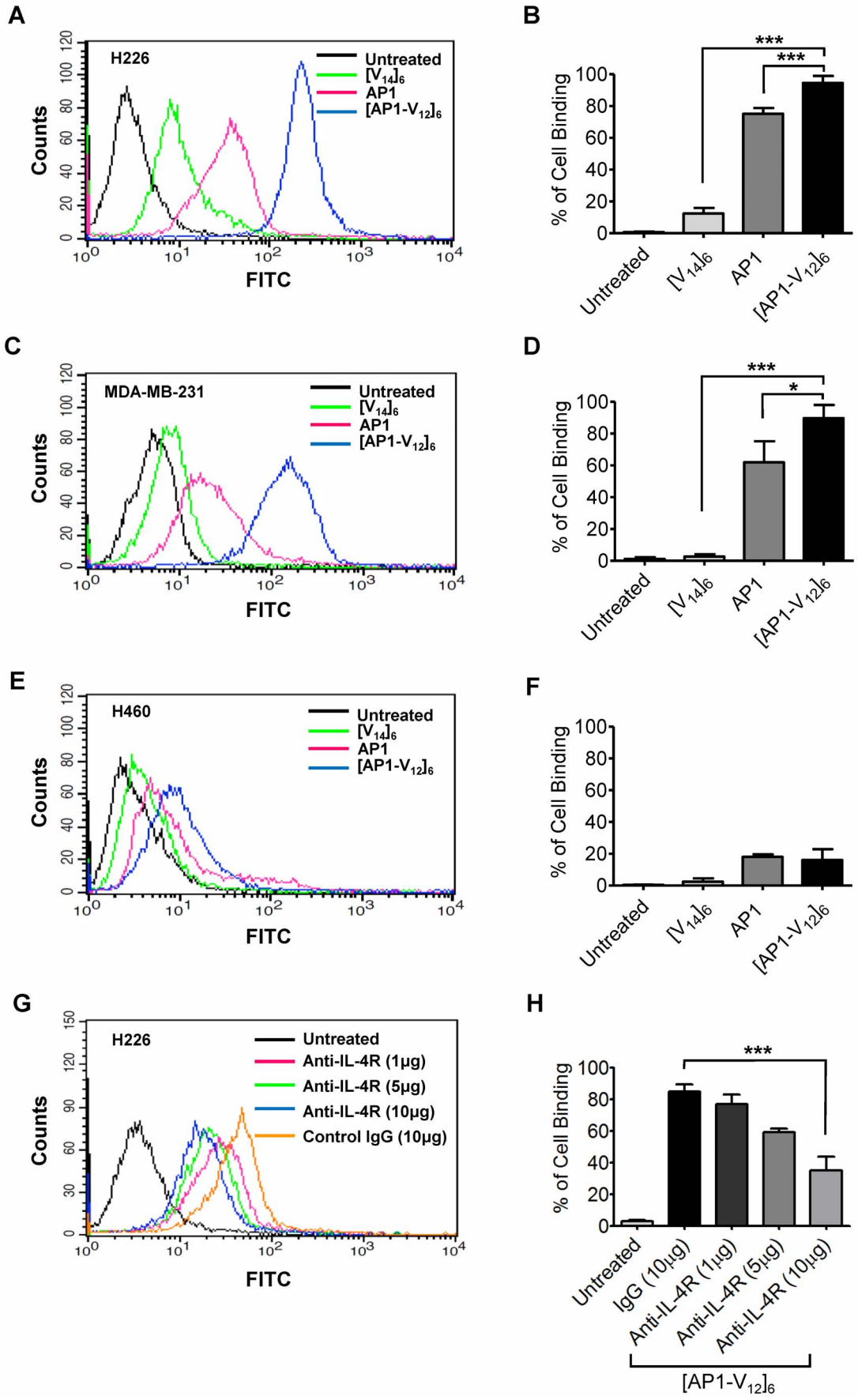
A
H226
Untreated
[V14]6
AP1
[AP1-V12]6
Counts
FITC
B
% of Cell Binding
***
***
Untreated
[V14]6
AP1
[AP1-V12]6
C
MDA-MB-231
Untreated
[V14]6
AP1
[AP1-V12]6
Counts
FITC
D
% of Cell Binding
***
*
Untreated
[V14]6
AP1
[AP1-V12]6
E
H460
Untreated
[V14]6
AP1
[AP1-V12]6
Counts
FITC
F
% of Cell Binding
Untreated
[V14]6
AP1
[AP1-V12]6
G
H226
Untreated
Anti-IL-4R (1μg)
Anti-IL-4R (5μg)
Anti-IL-4R (10μg)
Control IgG (10μg)
Counts
FITC
H
% of Cell Binding
***
Untreated
IgG (10μg)
Anti-IL-4R (1μg)
Anti-IL-4R (5μg)
Anti-IL-4R (10μg)
[AP1-V12]6

Figure 3. *In vitro* binding assays of $[V_{14}]_6$ and $[AP1\text{-}V_{12}]_6$ polymer. (A, B) H226, (C, D) MDA-MB-231 and (E, F) H460 cells were incubated with 10 μM of $[V_{14}]_6$, $[AP1\text{-}V_{12}]_6$ and AP1 for 1 h at 4°C. Cell binding was determined using flow cytometry. Histograms are representative of three independent experiments. Graphical bars (on right) represent the percent of Alexa 488 labeled polymer bound to cells as mean ±SD of data obtained from three separate experiments performed in triplicates. ***P<0.0001, **P<0.001, and *P<0.05, one-way ANOVA; n = 3. (G, H) H226 cells (3×10^5 cells) were pre- incubated with different concentrations (1, 5 and 10 μg/mL) of anti-IL-4 receptor antibody followed by 1 h incubation with 10 μM Alexa-labeled $[AP1\text{-}V_{12}]_6$ at 4°C. The cells were further suspended in 300 μL of PBS after washing and analyzed using flow cytometry. Histograms are representative of three independent experiments. Graphical bars represent the percent of Alexa 488 labeled polymer bound to cells as mean ±SD of data obtained from three separate experiments performed in triplicates. ***P<0.0001, One way ANOVA; n = 3.
doi:10.1371/journal.pone.0081891.g003

nonspecific effects of increased temperature. Further evidence for cellular localization of $[AP1\text{-}V_{12}]_6$ polymer on the cells were obtained by exploiting confocal microscopic Z-series images captured in sequential scanning mode, showed that the $[AP1\text{-}V_{12}]_6$ polymer was well distributed on the plasma membrane of H226 cells at 4°C (Fig. 4A, right panel) and internalized into cytoplasm when temperature was increased to 37°C (Fig. 4B, right panel).

Effect of $[AP1\text{-}V_{12}]_6$ polymer on proliferation of MDA-MB-231 cells

The cytotoxic effect of $[AP1\text{-}V_{12}]_6$ and $[V_{14}]_6$ polymer on proliferation of MDA-MB-231 cells was examined. Cytotoxicity of MDA-MB-231 cells after exposure to increasing concentration of $[AP1\text{-}V_{12}]_6$ and $[V_{14}]_6$ polymers shown similar pattern of cell viability and proliferation at different time intervals (Fig. 5A, B). Thus, the result indicated that both the polymers are nontoxic to the cancer cell.

We further investigated the effect of $[AP1\text{-}V_{12}]_6$ and $[V_{14}]_6$ polymer on IL-4 induced cell proliferation in MDA-MB-231 cells. IL-4 (10, 50 and 100 ng/ml) treated cells shown an increased in cell proliferation under low serum condition. The increase in cell proliferation upon IL-4 stimulation was brought to basal level after $[AP1\text{-}V_{12}]_6$ treatment, however cells continue to proliferate in $[V_{14}]_6$ and IL-4 treated cells (Fig. 5C). Thus, it is very clear that though $[AP1\text{-}V_{12}]_6$ has minimal effect on cell growth, it can inhibit IL-4 mediated cancer cells proliferation probably by binding the IL-4 receptor expressed on cancer cells.

Surface plasmon resonance analysis to check $[AP1\text{-}V_{12}]_6$ protein affinity for IL-4R

The kinetics of AP1 peptide and $[AP1\text{-}V_{12}]_6$ protein binding to the IL-4R were analyzed using surface plasmon resonance [31,32]. The $[AP1\text{-}V_{12}]_6$ polymer (Fig. 6A) showed higher binding affinity than the AP1 peptide (Fig. 6B) and $[V_{14}]_6$ (Fig. 6C). The equilibrium constants (K_D) of free AP1 peptide and $[AP1\text{-}V_{12}]_6$ protein were found to be $5.54\pm0.3\times10^{-3}$ and $2.07\pm0.3\times10^{-7}$, respectively (Table 1). Overall, the affinity of the $[AP1\text{-}V_{12}]_6$ polymer for the IL-4R was ~10000-fold higher than that of free AP1 peptide. No binding of $[V_{14}]_6$ was detected, even at concentrations as high as 1 μM. Thus, multivalent presentation of the targeting ligand AP1 on the ELP polymer backbone indeed increased the binding affinity towards the IL-4R.

In vivo imaging of $[AP1\text{-}V_{12}]_6$ polymer tumor targeting

The *in vivo* tumor-targeting efficiency of the $[AP1\text{-}V_{12}]_6$ polymer was studied using a near-infrared fluorescence (NIRF) live optical imaging system. *In vivo* fluorescence images taken at different time intervals showed that the $[AP1\text{-}V_{12}]_6$ polymer rapidly accumulated at tumor tissue (within a little as 10 min of injection) in MDA-MB-231 (Fig. 7A, B) breast cancer-bearing mice and was retained in tumor tissues for 24 h after injection. This specific targeting and sustained localization within tumors could provide sufficient time for $[AP1\text{-}V_{12}]_6$ polymer-conjugated drugs to exert their effects. In contrast, $[V_{14}]_6$ treated mice showed minimal fluorescence intensity at the tumors tissue and more nonspecific tissue localization. Six hours after injection, mice were sacrificed and *ex vivo* fluorescence images of tumor and excised organs were collected to evaluate the biodistribution of $[AP1\text{-}V_{12}]_6$ and $[V_{14}]_6$. $[AP1\text{-}V_{12}]_6$ fluorescence intensity was higher in the target tumor compared with that of $[V_{14}]_6$, confirming the increased tumor-targeting specificity and retention time of the AP1 peptide-modified ELP polymer. However, fluorescence intensity was also found to be strong in the liver and kidney of both targeted $[AP1\text{-}V_{12}]_6$ and non-targeted $[V_{14}]_6$ injected mice, indicating rapid metabolism and secretion in urine (Fig. 7C). An immunohistological examination of tumor tissue showed that abundant staining for $[AP1\text{-}V_{12}]_6$ was confined to the tumor tissue, consistent with our *in vivo* and *ex vivo* imaging results (Fig. 7D).

Discussion

Cancer cells express a number of cell surface and matrix proteins that mediate tumor growth, migration, invasion, and metastasis. Screening for ligands that specifically target these receptors represents an excellent cancer therapy strategy [33,34]. Initial studies using phage display technology discovered an IL-4R binding peptide (AP1) that was highly expressed on atherosclerotic plaques and cancer cells [16,17]. The AP1 peptide was found to bind the IL-4R with low affinity (i.e., micromolar dissociation constant), which means that more targeting peptide is necessary to achieve high receptor occupancy. To improve the binding affinity of AP1 as well as its avidity towards the IL-4 receptor, we incorporated multiple AP1 peptides into the ELP polymer.

The genetically encoded synthesis of $[AP1\text{-}V_{12}]_6$ allows easy synthesis of ligand-presenting ELP polymers and makes it possible to control their molecular weight and T_t to conform the requirements of physiological conditions. The ELP polymer backbone is capable of accommodating virtually any target specific ligand and can support multivalent presentation of target ligands without a change in its physical properties [35,36]. Many researchers have investigated the potential of ELP based incorporation of peptide as targeting moieties and cell penetrating peptide to improve the uptake by cancer cells [37,38]. Moreover there are many reports on application of diblock ELPs polymers consisting of a hydrophilic block and hydrophobic block capable of forming monodisperse spherical micelles above critical micelle temperature (CMT) for presentation of targeting ligands at their N-terminus site which enables multivalent presentation on their selective targets [36,39].

In this study for the first time we attempted to design ELP based multivalent targeting polymer by accommodating tandem repeat of highly specific IL-4R binding ligands, AP1 along the ELP polymer to improve its presentation towards IL-4R highly expressed cancer cells. Incorporation of AP1 on ELP elevated the T_t compared to ELP alone, likely due to the charged and polar surface residues present on AP1 [30]. Trabbic-Carlson et al. 2004 [30] already reported that the T_t of ELP fusion protein was negatively correlated with the fraction of hydrophobic area

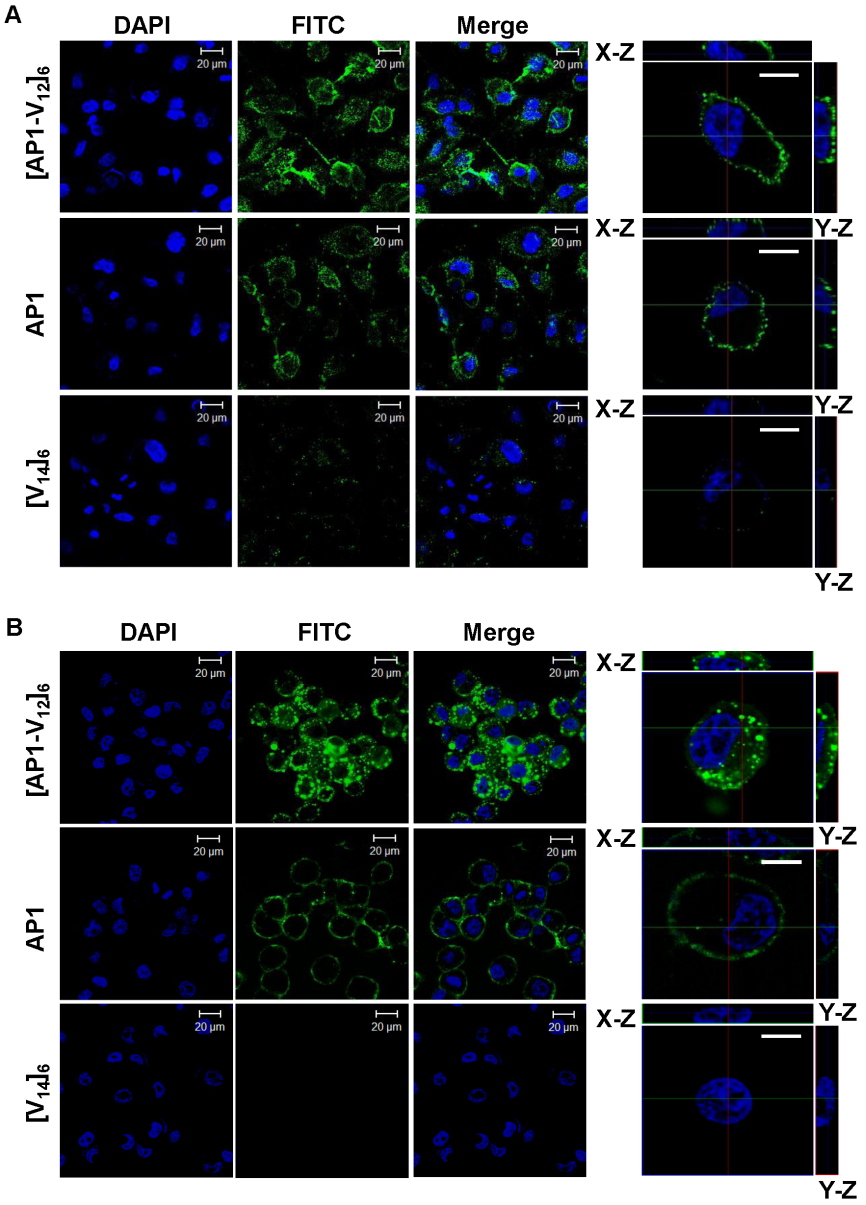

Figure 4. Analysis of cellular localization of $[AP1\text{-}V_{12}]_6$ polymer. Confocal laser scanning microscopic images of H226 cancer cells treated with 10 μM of $[AP1\text{-}V_{12}]_6$, AP1, or $[V_{14}]_6$ at (A) 4°C and (B) 37°C. Representative confocal images of three experiments (scale bar 20 μm). *Right panels*: Examination of $[AP1\text{-}V_{12}]_6$, AP1 and $[V_{14}]_6$ cellular location by Z-section scanning of confocal microscopic images. Representative confocal images of three experiments (scale bar 10 μm).
doi:10.1371/journal.pone.0081891.g004

presented on the surface of the fused folded protein. Proteins with relatively high hydrophobic solvent-accessible surface area depressed the inverse transition temperature of the fused ELP whereas proteins with more hydrophilic surfaces slightly increase elevated the transition temperature of the ELP fusion protein relative to that of the ELP.

The multivalent presentation of the targeting ligand AP1 on the ELP polymer backbone increased binding affinity ~10000-fold compared to the free AP1 peptide clearly denoted its augmentation in affinity and IL-4R interaction which is important for tumor targeting approach. *In vitro* studies further showed significantly higher binding of the $[AP1\text{-}V_{12}]_6$ polymer to IL-4R highly expressed H226 lung cancer and MDA-MB-231 human breast cancer cells than to IL-4R negative H460 cells. The increased cellular localization of the $[AP1\text{-}V_{12}]_6$ polymer over free AP1 peptide thus verifies the effectiveness of the multivalent, ELP-delivery strategy in improving tumor-targeting activity. Competitive inhibition of $[AP1\text{-}V_{12}]_6$ binding by different concentrations of anti-IL-4R antibody confirmed the specificity towards IL-4R.

Additionally confocal imaging results revealed the increased accumulation and uptake of $[AP1\text{-}V_{12}]_6$ polymer than $[V_{14}]_6$ control by IL-4R highly expressed tumor cells. Consistent with other findings [4,40], we believed that the significant enhancement in cellular uptake of thermally responsive $[AP1\text{-}V_{12}]_6$ polymer was due to increased temperature mediated phase transition which could possibly increase the exposure of IL-4R binding site to the cells thereby enhanced localization on cell surface and mediate cellular uptake.

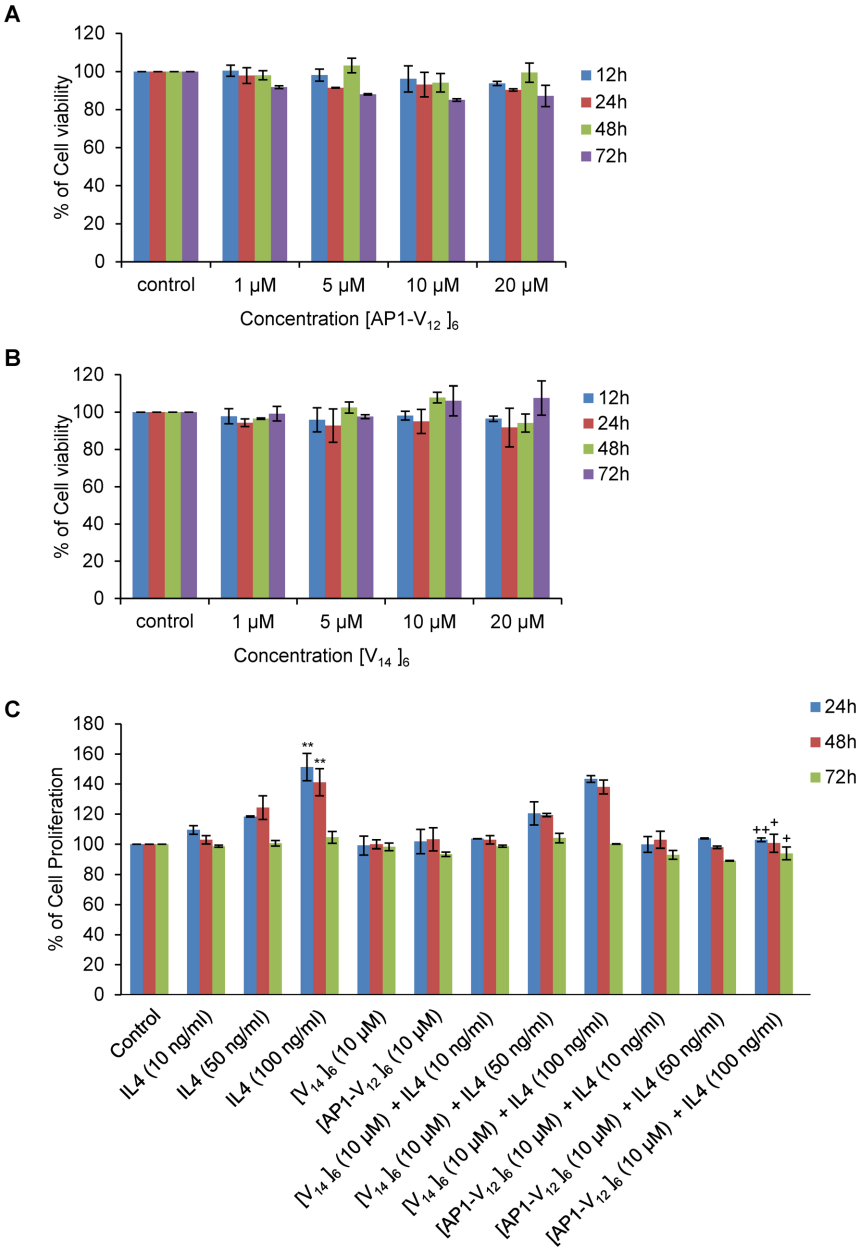

Figure 5. *In vitro* cell viability and proliferation assay. (A, B) MDA-MB-231 cells were plated in 96 well plates in serum (10% FBS) containing media and further treated with different concentration of $[AP1\text{-}V_{12}]_6$ and $[V_{14}]_6$ (1, 5, 10, 20 μM) for various time intervals (12, 24, 48, and 72 h). Cell viability was accessed by measuring WST-8 absorbance at 450 nm (n = 5) samples at different time intervals. The graph represents the percentage of cell viability in treated cells compared to control (untreated) cells. The result shown here is the representative data of 3 independent experiments. (C) For proliferation assay, MDA-MB-231 (2×10^3) cells were serum starved (1% FBS) for 16 h with or without different concentrations of IL-4. To check the effect of $[AP1\text{-}V_{12}]_6$ and $[V_{14}]_6$ on IL-4 stimulation, the cells were grown in low serum (1% FBS) media containing different concentration of IL-4 (10, 50, 100 ng/ml) and $[AP1\text{-}V_{12}]_6$ and $[V_{14}]_6$ (10 μM) for 24, 48, and 72 h. Cell proliferation was analyzed by measuring the WST-8 absorbance at 450 nm (n = 5 samples). The graph represents the percentage of cell viability in treated cells compared to control (untreated) cells. The result shown here is the representative data of 3 independent experiments. A t-test was performed to determine the significance of various groups after IL-4 and polymer treatments. Control versus IL-4 (100 ng/ml), * = $P<0.05$ and ** = $P<0.001$, IL-4 (100 ng/ml) versus $[AP1\text{-}V_{12}]_6$ + IL-4 (100 ng/ml), + = $P<0.05$ and ++ = $P<0.001$.
doi:10.1371/journal.pone.0081891.g005

Previous studies have suggested that IL-4 can promote proliferation of various cancer cells of different origin under nutrient depletion stress condition [41]. The experiments were performed to examine the modulating effect of our $[AP1\text{-}V_{12}]_6$ polymer on MDA-MB231 cell proliferation in presence or absence of IL-4. Our cytotoxicity assay revealed that both $[AP1\text{-}V_{12}]_6$ and $[V_{14}]_6$ polymers are nontoxic to cancer cell, as both polymers have least effect on cell viability or proliferation in absence of external IL-4 supplements. However, under nutrient depletion condition only $[AP1\text{-}V_{12}]_6$ but not $[V_{14}]_6$ shown inhibition of cell growth in presence of IL-4. Thus our result implicated that $[AP1\text{-}V_{12}]_6$ might inhibit IL-4 mediated cancer cells proliferation probably by binding the IL-4 receptor expressed on cancer cells.

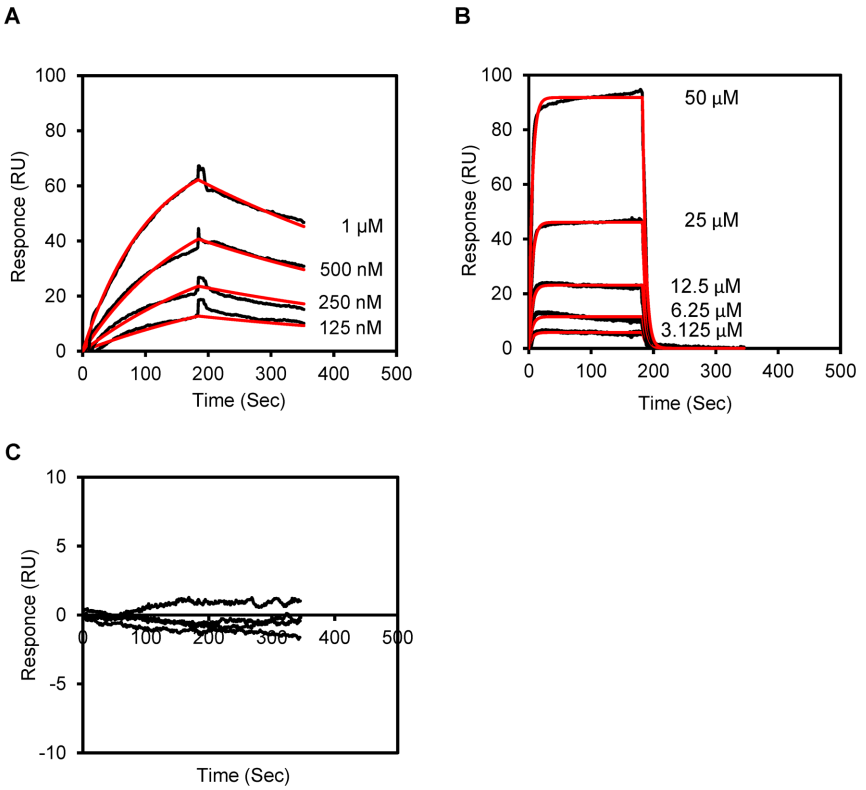

Figure 6. IL-4 R binding affinity of $[AP1\text{-}V_{12}]_6$ polymer. Determination of binding kinetics. Normalized (A) $[AP1\text{-}V_{12}]_6$ protein (125 nM - 1 μM), (B) AP1 peptide (3.125 - 50 μM) and (C) $[V_{14}]_6$ (1 μM) binding curves (black line) with fits (red line) obtained using Scrubber 2. Histograms are representative of three independent experiments.
doi:10.1371/journal.pone.0081891.g006

Determination of targeting efficacy *in vivo* is very important for verifying precise homing of $[AP1\text{-}V_{12}]_6$ to tumor tissue. In this study we have used MDA-MB-231 tumor xenograft mouse model because of rapid propagation of cells subcutaneously, re-forming into solid tumors within a short duration. *In vivo* fluorescence imaging of the tumor site at different times after injection confirmed higher levels of fluorescence signals of $[AP1\text{-}V_{12}]_6$ in MDA-MB-231 tumor-bearing mice, an observation that was further confirmed by immunohistological examinations of frozen tissue sections. Previous *in vivo* studies using pH-responsive, AP1-containing micelles demonstrated gradual binding to tumor tissue with maximum intensity at 24 h [18]. Notably, our genetically engineered ELP-based AP1 polymers further enhanced tumor targeting ability, showing high tumor accumulation that was evident as early as 10 min after intravenous injection, peaked after about 6 h, and was maintained up to 24 h (Fig. 7). With the exception of kidney and liver, fluorescence levels were negligible in off-target organs, including the lung, spleen, and heart. Even though our designed the $[AP1\text{-}V_{12}]_6$ polymer has T_t just above the physiological body temperature, which is preferable for clinical applications [42], T_t of $[V_{14}]_6$ control is found to be relatively lower than the $[AP1\text{-}V_{12}]_6$. However, the difference in T_t was not an emphasis due to application of lesser concentration of non-targeting and targeting polymer during *in vivo* experiments. Besides, $[V_{14}]_6$ control was found to accumulate in various organs post intravenous injection except in the tumor tissue unlike the case of $[AP1\text{-}V_{12}]_6$ injected groups with precise localization to tumor tissue. Collectively, these findings highlight the promise of our $[AP1\text{-}V_{12}]_6$ polymer as a candidate macromolecular drug delivery system. Although our ELP-based polymers can target only IL-4R overexpressed cancer cells, many tumor of different origin have been reported to highly expressed IL-4R [19–22] and thus our designed polymer can be used as a potent drug carrier for various targeted cancer therapies.

Table 1. Determination of binding kinetics.

	k_{on} ($M^{-1}S^{-1}$)	k_{off} (S^{-1})	K_D(M^{-1})
$[AP1\text{-}V_{12}]_6$	$5.81\pm1.5\times10^{3}$	$1.25\pm0.5\times10^{-3}$	$2.07\pm0.3\times10^{-7}$
AP1	$3.5\pm0.5\times10^{1}$	$1.70\pm0.2\times10^{-1}$	$5.54\pm0.3\times10^{-3}$

Association (k_{on}), dissociation (k_{off}) and equilibrium (K_D) constants of $[AP1\text{-}V_{12}]_6$ and AP1 peptide from kinetic fits obtained from Scrubber 2. The data ±SD obtained for three independent experiments (n = 3).
doi:10.1371/journal.pone.0081891.t001

The strategy of designing macromolecular carrier systems with multivalent ligand presentation for targeting surface molecules displayed on solid tumors has clear value in clinical applications. Because of relatively simple and novel synthetic process and the ability to use multivalent peptides and targeting moieties, we proposed a method which is distinctive and explore a new arena of multivalent cancer targeting. Although our multivalent targeting system exhibited effective tumor accumulation, further study is needed to realize the promise of ELP-based targeting polymers as carriers for delivering chemotherapeutic agents and therapeutic peptides.

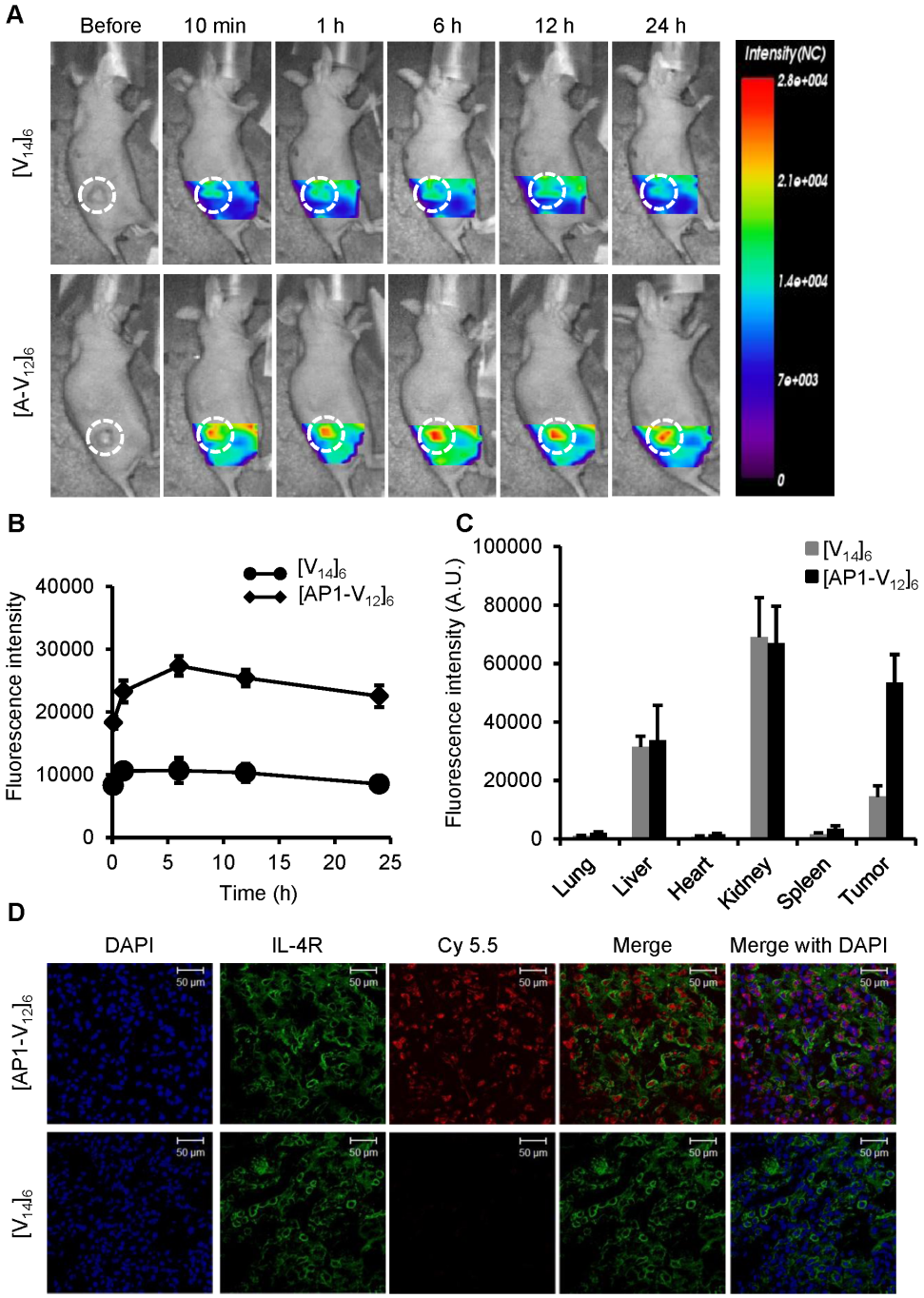

Figure 7. *In vivo, ex vivo* imaging and biodistribution of $[AP1\text{-}V_{12}]_6$ polymers. (A) Cy5.5-labeled $[V_{14}]_6$ and $[AP1\text{-}V_{12}]_6$ (8 mg/kg) were intravenously injected into MDA-MB-231 tumor xenografted nude mice. Biodistribution was determined by collecting *in vivo* fluorescence images at different time points. Scale bar indicates normalized fluorescence intensity (NC). Representative optical images of three experiments. (B) Quantitation of fluorescence intensities in tumor sites at respective time points (n = 3). (C) Analysis of fluorescence intensities for tumors and organs from *ex vivo* images (n = 3). (D) Histological analysis of $[AP1\text{-}V_{12}]_6$ polymer (red) localization in tumors. Nuclei were stained with DAPI (blue), and IL-4R expression on cells was visualized by anti-IL-4 receptor antibody staining (green). Representative confocal images of three experiments (scale bar 50 μm).
doi:10.1371/journal.pone.0081891.g007

Supporting Information

Figure S1 Agarose gel electrophoresis of (A) $[V_{14}]_n$ and (B) $[AP1\text{-}V_{12}]_n$, (n = 1, 2, 4, 5 and 6) represents the number of monomer-gene repeats, visualized by ethidium bromide staining. The left lane contains a 1-kb DNA size marker. pRSET vectors containing ELP genes were double digested with *Bam*H I and *Hin*D III, producing two bands corresponding to the vector (2900 bp) and variable-sized ELPs. The number of monomer-gene repeats (1, 2, 4, 5 and 6) is labeled on top, and expected ELP sizes are given on the right. (C) Partial sequence consists of *Sfi* I site, used for pET25b+ vector modification. (D) $[V_{14}]_6$ and (E) $[AP1\text{-}V_{12}]_6$ genes digested with *Pfl*M I and *Bgl* I were ligated to *Sfi* I-digested, modified pET 25b+

vector. The sizes of DNAs were confirmed by double digestion with *Nde* I and *Hin*D III. Two bands corresponding to the vector (5547 bp) and ELP gene (1294 bp) were produced.
(TIFF)

Figure S2 Confocal microscopic images of MDA-MB-231 cells treated with 10 μM of $[AP1\text{-}V_{12}]_6$, AP1, or $[V_{14}]_6$ for 1 h at (A) 4°C and (B) 37°C. Unbound peptides were washed out with PBS, and cells were fixed with 4% paraformaldehyde. Cell nuclei were stained with DAPI. Representative confocal images of three experiments (scale bar 20 μm).
(TIFF)

Figure S3 Confocal microscopic images H460 cells treated with 10 μM of $[AP1\text{-}V_{12}]_6$, AP1, or $[V_{14}]_6$ for 1 h at (A) 4°C and (B) 37°C. Cells were fixed with 4% paraformaldehyde and cell nuclei were stained with DAPI. Representative confocal images of three experiments (scale bar 20 μm).
(TIFF)

Acknowledgments

The authors are grateful to Ji-yeon Jeong and Chi Lianhua for technical assistance.

Author Contributions

Conceived and designed the experiments: VS RWP BHL. Performed the experiments: VS EAC SMB TDS SJK. Analyzed the data: VS TDS WBJ SK RWP. Contributed reagents/materials/analysis tools: SJK. Wrote the paper: VS RWP.

References

1. Duncan R (2006) Polymer conjugates as anticancer nanomedicines. Nat Rev Cancer 6(9): 688–701.
2. Dreher MR, Raucher D, Balu N, Michael Colvin O, Ludeman SM, et al. (2003) Evaluation of an elastin-like polypeptide-doxorubicin conjugate for cancer therapy. J Control Release 91(1–2): 31–43.
3. Gene L, Bidwell III, Izabela F, Waldemar P, Raucher D (2007) Development of elastin-like polypeptide for thermally targeted delivery of doxorubicin. Biochemical Pharmacology 73: 620–631.
4. Gene L, Bidwell III, Drazen R (2005) Application of thermally responsive polypeptides directed against c-Myc transcriptional function for cancer therapy. Mol Cancer Ther 4(7): 1076–1085.
5. Shamji MF, Chen J, Friedman AH, Richardson WJ, Chilkoti A, et al. (2008) Synthesis and characterization of a thermally-responsive tumor necrosis factor antagonist. J Control Release 129 (3): 179–186.
6. Urry DW, Parker TM, Reid MC, Gowda DC (1991) Biocompatibility of the bioelastic materials, poly (gvgvp) and its gamma-irradiation cross-linked matrix - summary of generic biological test-results. J Bioact Compat Polym 6 (3): 263–282.
7. Shamji MF, Betre H, Kraus VB, Chen J, Chilkoti A, et al. (2007) Development and characterization of a fusion protein between thermally responsive elastin-like polypeptide and interleukin-1 receptor antagonist: sustained release of a local anti-inflammatory therapeutic. Arthritis Rheum 56 (11): 3650–3661.
8. Urry DW, Luan CH, Parker TM, Gowda DC, Prasad KU, et al. (1991) Temperature of Polypeptide Inverse Temperature Transition Depends on Mean Residue Hydrophobicity. J Am Chem Soc 113: 4346–8.
9. Tatham AS, Shewry PR (2000) Elastomericproteins: biological roles, structures and mechanisms. Trends Biochem Sci 25: 567–71.
10. Meyer DE, Chilkoti A (2004) Quantification of the effects of chain length and concentration on the thermal behavior of elastin-like polypeptides. Biomacromolecules 5 (3): 846–851.
11. Meyer DE, Chilkoti A (2002) Genetically encoded synthesis of protein-based polymers with precisely specified molecular weight and sequence by recursive directional ligation: examples from the elastin-like polypeptide system. Biomacromolecules 3 (2): 357–367.
12. Urry DW (1992) Free energy transduction in polypeptides and proteins based on inverse temperature transitions. Prog Biophys Mol Biol 57: 23–57.
13. Urry DW (1997) Physical chemistry of biological free energy transduction as demonstrated by elastic protein-based polymers. J Phys Chem B 101: 11007–11028.
14. Meyer DE, Chilkoti A (1999) Purification of recombinant proteins by fusion with thermally responsive polypeptides. Nat Biotechnol 17 (11): 1112–1115.
15. Trabbic-Carlson K, Liu L, Kim B, Chilkoti A (2004) Expression and purification of recombinant protein from Escherichia coli: comparison of an elastin-like polypeptide fusion with an oligohistidine fusion. Protein Sci 13 (12): 3274–3284.
16. Hong HY, Lee HY, Kwak W, Yoo J, Na MH, et al. (2008) Phage display selection of peptides that home to atherosclerotic plaques: IL-4 receptor as a candidate target in atherosclerosis. J Cell Mol Med 12: 2003–2014.
17. Park K, Hong HY, Moon HJ, Lee BH, Kim IS, et al. (2008) A new atherosclerotic lesion probe based on hydrophobically modified chitosan nanoparticles functionalized by the atherosclerotic plaque targeted peptides. J Control Release 128: 217–223.
18. Wu XL, Kim JH, Koo H, Bae SM, Shin H, et al. (2010) Tumor-Targeting Peptide Conjugated pH-Responsive Micelles as a Potential Drug Carrier for Cancer Therapy. Bioconjugate Chem 21: 208–213.
19. Obiri NI, Hillman GG, Haas GP, Sud S, Puri RK (1993) Expression of high affinity interleukin-4 receptors on human renal cell carcinoma cells and inhibition of cell growth *in vitro* by interleukin 4. J Clin Invest 91: 88–93.
20. Obiri NI, Siegel JP, Varricchio F, Puri RK (1994) Expression of high-affinity IL-4 receptors on human melanoma, ovarian and breast carcinoma cells. Clin Exp Immunol 95: 148–155.
21. Husain SR, Gill P, Kreitman RJ, Pastan I, Puri RK (1997) Interleukin-4 receptor expression on AIDS-associated Kaposi's sarcoma cells and their targeting by a chimeric protein comprised of circularly permuted interleukin-4 and *Pseudomonas* exotoxin. Mol Med 3: 327–328.
22. Kawakami K, Leland P, Puri RK (2000) Structure, function, and targeting of interleukin 4 receptors on human head and neck cancer cells. Cancer Res 60: 2981–2987.
23. Todaro M, Lombardo Y, Francipane MG, Perez Alea M, Cammareri P, et al. (2008) Cell Apoptosis resistance in epithelial tumors is mediated by tumor-cell-derived interleukin-4. Cell Death Differ 15: 762–772.
24. Conticello C, Pedini F, Zeuner A, Patti M, Zerilli M, et al. (2004) IL-4 Protects Tumor Cells from Anti-CD95 and Chemotherapeutic Agents via Up-Regulation of Antiapoptotic Proteins. J Immunol 172 (9): 5467–5477.
25. Liu S, Maheshwari R, Kiick K (2009) Polymer-Based Therapeutics. Macromolecules 42 (1): pp 3–13.
26. Jeon WB, Park BH, Wei J, Park RW (2011) Stimulation of fibroblasts and neuroblasts on a biomimetic extracellular matrix consisting of tandem repeats of the elastic VGVPG domain and RGD motif. J Biomed Mat Res 97 (2): 152–7.
27. Jeon WB, Park BH, Choi SK, Lee KM, Park JK (2012) Functional enhancement of neuronal cell behaviors and differentiation by elastin- mimetic recombinant protein presenting Arg-Gly-Asp peptides. BMC Biotechnology 12: 61.
28. Kawakami M, Kawakami K, Vitaly A, Stepensky RA, et al. (2002) Interleukin 4 Receptor on Human Lung Cancer: A Molecular Target for Cytotoxin Therapy. Clin Cancer Res 8: 3503–3511.
29. He X, Na MH, Kim JS, Lee GY, Park JY, et al. (2011) A Novel Peptide Probe for Imaging and Targeted Delivery of Liposomal Doxorubicin to Lung Tumor. Mol Pharm 8: 430–438.
30. Carlson KT, Meyer DE, Liu L, Piervincenzi R, Nath N, et al. (2004) Effect of protein fusion on the transition temperature of an environmentally responsive elastin-like polypeptide: a role for surface hydrophobicity? Protein Engineering. Design and Selection 17: no. 1 pp, 57±66.
31. Andrews AL, Holloway JW, Holgate ST, Davies DE (2006) IL-4 Receptor α is an Important Modulator of IL-4 and IL-13 Receptor Binding: Implications for the Development of Therapeutic Targets. J Immunol 176: 7456–7461.
32. McElroy CA, Dohm JA, Scott TR (2009) Walsh Structural and Biophysical Studies of the Human IL-7/IL-7Rα Complex. Structure 17: 54–65.
33. Ruoslahti E, Sangeeta N, Bhatia MJ (2010) Sailor Targeting of drugs and nanoparticles to tumors. J Cell Biol 188 (6): 759–768.
34. Li ZJ, Cho CH (2012) Peptides as targeting probes against tumor vasculature for diagnosis and drug delivery. J Transl Med 10: (Suppl 1) S1.
35. Gene L, Bidwell III, Perkins E, Raucher D (2012) A thermally targeted c-Myc inhibitory polypeptide inhibits breast tumor growth. Cancer Letters 319: 136–143.
36. Simnick AJ, Amiram M, Liu W, Hanna G, Mark W, et al. (2011) In vivo tumor targeting by a NGR-decorated micelle of a recombinant diblock copolypeptide. J Control Release 155: 144–151.
37. Wender PA, Mitchell DJ, Pattabiraman K, Pelkey ET, Steinman L, et al. (2000) The design, synthesis, and evaluation of molecules that enable or enhance cellular uptake: Peptoid molecular transporters. Proc Natl Acad Sci U S A 97: pp 13003–13008.
38. Massodi I, Bidwell GL, Raucher D (2005) Evaluation of cell penetrating peptides fused to elastin-like polypeptide for drug delivery. J Control Release 108 (2–3): 396–408.
39. Hassouneh W, Fischer K, MacEwan SR, Branscheid R, Fu CL, et al. (2012) Unexpected multivalent display of proteins by temperature triggered self-assembly of elastin like polypeptide block copolymers. Biomacromolecules 13: 1598–1605.
40. Raucher D, Chilkoti A (2001) Enhanced uptake of a thermally responsive polypeptide by tumor cells in response to its hyperthermia-mediated phase transition. Cancer Res 61: 7163–7170.

41. Roca H, Craig MJ, Ying C, Varsos ZS, Czamieski P, et al. (2012) IL-4 Induces Proliferation in Prostate Cancer PC3 Cells Under Nutrient-Depletion Through the Activation of the JNK-Pathway and Survivin Up- Regulation. J Cell Biochem 113: 1569–1580.

42. Yuan F, Dellian M, Fukumura D (1995) Vascular Permeability in a Human Tumor Xenograft: Molecular Size Dependence and Cutoff Size. Cancer Res 55: 3752–3756.